ASTROPHYSICS

(stellar atmospheres, interacting binary systems, variable stars)

https://doi.org/10.18524/1810-4215.2023.36.290774

THE PROBLEM OF OBTAINING COMBINED GAMMA AND OPTICAL DETECTORS FOR THE REGISTRATION OF FAST NUCLEAR PROCESSES

Marko D. Doikov

Faculty of Physics and Technologies, Plovdiv University "Paisii Hilendarski",

Plovdiv, Bulgaria, *marik.doikov@gmail.com*

ABSTRACT. The physical and technical aspects of the registration of fast physical processes involving nuclear transformations with the help of binary detectors in the γ- and optical ranges are considered We chose a semiconducting perovskite crystal $CsPbBr_3$ as the main element of the detector. Have been presented with geometrical and technologically usable parameters of the $CsPbBr_3$ crystal for its implementations in nuclear medicine, geophysics and astrophysics. One of the objects that allow testing of the developed high-speed spectrographic equipment are lightning discharges in the atmospheres of planets, including the Earth. The thermonuclear nature of γ-bursts detected during thunderstorms was revealed by their spectra. The paper shows the role of the corresponding channels involving high-energy protons and α-particles, leading to the formation of ${}^{11}_{6}C$, ${}^{13}_{7}N$, and ${}^{15}_{8}O$ isotopes. The registration of the γ-spectrum of the flash and its evolution allowed to estimate the character, energy and time scales of the processes necessary for the design and manufacture of multipurpose measuring complexes by us. The inclusion of γ-spectra in the consideration allowed to estimate the correlation between the maximum currents of particles and the productivity of γ-rays. In the experiments planned by us, the magnetic field fluctuations caused by currents are simultaneously recorded by highly sensitive magnetic field detectors. The height of the building of the Faculty of Physics in Smolyan, Bulgaria, is 900 meters above sea level. This makes it possible to place the measuring complex as close as possible to the sources of hard radiation and to carry out measurements in the immediate vicinity. Unlike distant space objects, the perovskite detector registers the positions themselves. This makes it possible to use the methods of positron γ-spectroscopy and accurately determine the parameters of local currents. The technological parameters of the device were determined.

A simulation model was created in Simulink MATLAB, LabVIEW with synchronization of the operation of the listed spectrographs. The characteristic shape of the signal formed by individual γ-quanta with the parameters of the Gaussian function and the total number of these quanta are calculated. The degree of mathematical blinding of neighboring Gaussian functions and its influence on the structure of the final spectrogram in the form of an autocorrelation function is estimated.

The similarity of the time scales of thermonuclear explosion processes on white dwarfs (WD) and the processes of synthesis of ${}^{11}_{6}C$, ${}^{13}_{7}N$, and ${}^{15}_{8}O$ isotopes in the flash head is determined. It is concluded that it is expedient to create a robotic network of lightning observation stations similar to the meteor patrol at the I. I. Mechnikov National University of Ukraine.

Keywords: γ-ray spectroscopy; CsPbBr3 detectors, ionization rays, higher speed interface, rapid nuclear transformation diagnostics, signal-noise relation.

АНОТАЦІЯ. Підвищення чутливості та розширення спектрального діапазону детекторів γ-випромінювання за останні десять років призвело до значних успіхів у галузі природничих і технічних наук. Однією з визначних подій у цій галузі є поява перших повідомлень про створення комерційних кристалів $CsPbBr_3$ у 2016 році, а також заявлена можливість їх застосування в ядерній медицині, геофізиці та астрофізиці. На сьогодні відомо, що кристали $CsPbBr_3$ є напівпровідниками з великим середнім атомним номером 57,35 а. м. u. Ширина забороненої зони 4,5 еВ легко регулюється під час виготовлення кристала та під дією зовнішнього електричного поля. Енергія утворення електронно-діркової пари становить 5,3 еВ. Це дозволяє використовувати спектроскопічне обладнання в експедиційних умовах без використання охолодження. Високі значення добутку швидкості рухливості зарядів μ на час їх життя τ складають $\mu\tau = 8 \cdot 10^{-4}$ см2/В. В даний час середній розмір кристала становить 3x3x0,9 мм. У роботи отримано, що у разі поперечних перерізів детекторів S=9mm^2 отримуються високоточні деталізовані рентгенівські та γ-спектри в діапазоні енергій 0,01 – 1 МеВ. У цьому випадку корпус детектора ефективно поглинає падаючі кванти і має високу продуктивність електронно-діркових пар. У разі енергій, перевищуючих 1,022 МеВ, спектр падаючого випромінювання спотворюється спільною дією, пов'язаною з появою електрон-позитронних пар в інтенсивному навколо ядерному полі кристалічних атомів, розсіюванням Комптона γ-квантів, атомним фотоефектом і когерентним розсіянням квантів на електронах, власною люмінесценцією, оже-електронами. Автором використано колекція емпіричних вимірювань лінійного коефіцієнта поглинання γ-випромінювання, які дозволяють

уникнути непотрібних складних розрахунків і експериментів. Виражена нелінійність k_E дозволяє вибрати оптимальну геометрію детекторів. Зроблено розрахунок із відношення поглинених даного типу γ-квантів до енергії утворення однієї електронно-діркової пари 5,3 еВ. Незважаючи на уявні проблеми теоретичного підходу та вироблення кристалів, точність реєстрації розглянутими детекторами вже досягла кількох процентів. В основній частині статті розглянуто роботу електроніки у режимі підрахунку імпульсів, аналіз форми імпульсів і їх вплив на результуючий спектр . У наших попередніх роботах ми розраховували потоки γ-квантів у вибухових термоядерних процесах. На 1 см^2 детектора від астрофізичного об'єкта за 20 мкс. потрапило 180 фотонів з енергією не більше 10 МеВ. Тому необхідно, щоб детектований γ-спектр міг містить безперервні фонові кванти та лінії випромінювання. Запропоновано алгоритм виділення ліній і неперервного спектра. Зроблено схемні рішення для емуляції генератора сигналів необхідної форми, що утворюються після проходження квантів жорсткого рентгенівського та м'якого γ-випромінювання скрізь кристал $CsPbBr_3$ Надано увагу перспективам розвитку теорії та практики бінарних детекторів нового покоління.

Ключові слова: γ-спектроскопія; Детектори CsPbBr3, іонізаційні промені, високошвидкісний інтерфейс, швидка діагностика ядерних перетворень, зв'язок сигнал-шум.

1. Introduction

The increase in sensitivity and the extension of the spectral range of γ-band detectors in the last decade has led to significant advances in the field of natural and engineering sciences. One of the remarkable events in this field is the appearance of the first reports on the creation of commercial crystals of CsPbBr3 perovskite in 2016. It also explained the possibility of their application in nuclear medicine, geophysics, and astrophysics.

At present, it is known (Liu et al., 2022) that$CsPbBr_3$ crystals are semiconductors with a large average atomic number of 57.35 a. m. u. The band gap of 4.5 eV can be easily tuned during the crystal growth and under the action of an external electric field. The energy of electron-hole pair formation is 5.3 eV. This allows the use of spectroscopic instruments in the field without the need for cooling. High values of the product of the mobility rate μ of the charges and their lifetime τ are $\mu\tau = 8\cdot10^{-4}$ cm^2/V. Currently, the average crystal size is 3x3x0.9 mm. Note that the detector cross section is $S = 9\ mm^2$. Detectors with reduced dimensions make it possible to obtain high-precision, detailed X-rays and γ-spectra in the energy range 0.01 – 1.0 MeV. In this case, the detector body effectively absorbs the incident quanta and has high electron-hole pair productivity.

At energies above 1.022 MeV, the incident emission spectrum is distorted by the combined action associated with the appearance of electron-positron pairs in an intense near-nuclear field of crystal atoms, Compton scattering of γ quanta, atomic photoelectric effect and coherent scattering of quanta by electrons, intrinsic luminescence, Auger electrons, etc. Therefore, measurements of the linear absorption coefficient of γ radiation k_E allow to avoid unnecessary complex calculations and experiments.

The expressed nonlinear character k_E (Liu et al., 2022, Fig. 2 C) allows to choose the optimal geometry of the detectors. In the future, we will be guided by the absorbed energy according to the empirical values of k_E. And only for the energy intervals in which one of the above mechanisms predominates, we will use the values of the exact theoretical cross sections calculated in our previous works. Calculation from the ratio of the absorbed γ-quanta of a given type to the formation energy of an electron-hole pair of 5.3 eV. Despite the apparent roughness of the approach, the accuracy of registration by the marked detectors has already reached several percent (Liu et al., 2022; Lopes et al., 2020). The operation of the considered detectors in pulse-counting mode, saturation modes, and their calibration in section 2. In our previous work, we calculated the fluxes of γ quarks in fast, explosive thermonuclear processes. 180 photons with energies not exceeding 10 MeV were fired from an astrophysical object onto $1cm^2$ of the detector in 20 μs (Doikov D., 2022). The γ spectrum recorded by the detector contains continuous background quanta and emission lines. An algorithm to select the lines and the continuous spectrum is proposed. In section 3, circuit solutions are given for emulating the signal generator of the required shape, formed after the passage of hard x-ray and soft γ-radiation quanta through the CsPbBr3 crystal. The discussion is devoted to the prospects for the development of the theory and practice of the new generation of binary detectors.

2. The selection of the signal type from test objects

The close binary systems with white dwarfs (WD) and companion stars with a Sun-like chemical composition. So-called Cataclysmic Variable Stars (CVs). The accretion from the companion star to the surface of the WD through its hard magnetic field (1000 T) creates the conditions for the production of the induced γ-ray (Doikov D., 2022). The theoretical background γ-ray production forms 10-20 quants at the localization point of the Earth and the space closest to it. The possible thermonuclear explosion produced in formal Earth detector γ-ray fluxes is 100 quants/cm^2/s at time intervals $\Delta\tau \approx 10^{-4}s$. In AM Her type CVs these events repeat several times a year. The use of the considered detector spectrographs in monitoring mode allows the registration of random events of explosive origin in space. In such conditions, the development of binary detector-spectrographs in the γ and optical spectral ranges allows for an increase in the probability of detection of explosion precursors. Other astrophysical objects are not considered in this section because the physical processes in them are more complex, both in time and in the structure of the spectra.

Relaxation times $\Delta\tau_{rel}$ of pulse formation limited by Δτ. Strictly speaking, $\Delta\tau_{rel} \leq \Delta\tau/100$. During this time, a γ quantum must pass through a 0.9 mm thick crystal, transfer energy to the valence electrons, and they must pass through the band gap. As noted in the introduction, the average number$N_{\gamma e}$ of electron-hole pairs from a single γ-quantum will be

$$N_{\gamma e} = \frac{E_\gamma\left(1-e^{-\kappa_\gamma d}\right)}{5{,}3\ eV}\ . \qquad (1)$$

Where $E_\gamma$is the energy of the γ quantum, κ_γ is the coefficient of linear monochromatic extinction. The dependence of $\kappa_\gamma$on γ-quantum energies is presented in (Liu et al., 2022, Fig. 2, B), using data from NIST USA (19 references in this paper). In Fig. 1 we have shown the dependence of $N_{\gamma e}$ on the γ-ray energy E_γ. The saturation of $N_{\gamma e}$only denotes the fact that the radiation length of γ-quats is more from crestal depth.

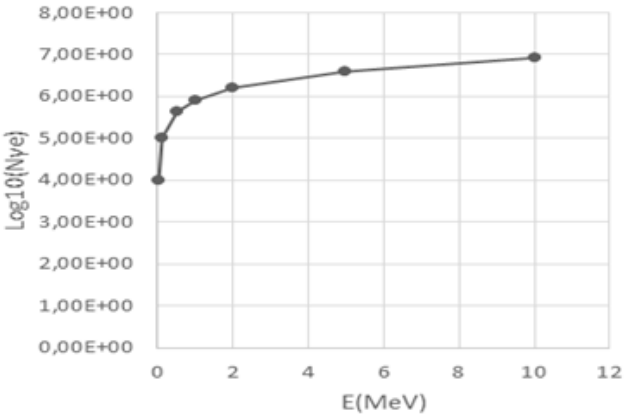

Figure 1: Dependence of the number of injected electrons in the conductivity zone log10($N_{\gamma e}$)) from the γ-ray energy E(MeV).

3. Earth atmosphere

In recent years, the demand for increasing the sensitivity of γ-spectrographs for practical needs in many branches of practical activity has increased sharply. In this work, the main attention is paid to the selection of available equipment and the development of software for monitoring fast processes in plasma with the presence of reactive electrons, protons, and α-particles. In last year's studies, it was shown that under certain conditions, the presence of flows of charged particles accelerated to relativistic speeds in plasma leads to radiative losses of kinetic energy for radiation. The article (Doikov D., 2022) describes in detail the sequence of radiation losses as a function of time and energy regimes. In order to develop the necessary equipment, in our work we calculated the time frame for the processes of induction of hard radiation and the values of the fluxes. Testing such equipment for astrophysical purposes is difficult due to the fact that the Earth's atmosphere absorbs the hard radiation of interest to us. Therefore, alternative sources were sought to calibrate the multichannel spectrograph. A suitable source of broad-spectrum radiation is lightning. It was found that the time intervals for the formation of hard and optical radiation can be divided into 3 stages.

In the first stage, γ-rays appear before the onset of an optical flare. Its duration is 1-10 μs. In the second stage, during an optical flare, a broad spectrum of radiation is observed within 10-100 milliseconds. In the third stage, after the disappearance of the optical radiation, γ-rays are observed for a few more seconds. In contrast to astrophysical problems, the measuring equipment during such a calibration must include a magnetometer and a radio rangefinder. The latter two devices available on the market have a high sensitivity and a low affordable price. The main task is to switch and synchronize the operation of the optical and γ-spectrographs. The accuracy of synchronization of individual elements of a multichannel spectrograph in monitoring mode should be 1-10 ns. Before manufacturing a spectrograph, it is necessary to simulate the registration processes with standard devices placed in the LabVIEW environment. Each individual signal is converted into an equivalent rectangular shape. In reality, the actual shape of the current pulse of the generated signal after the interaction of a hard radiation quantum with the perovskite material is well approximated by the Gaussian function.

The conversion to a square pulse is done in the INTEGRATOR. As with optical and γ-spectrographs, it is necessary to know the resolution and the signal-to-noise ratio. This year's articles have already explained that the signal-to-noise ratio is (80pA / 20pA). And the resolution is already approaching 1 KeV. It is also important to note that the fight against noise when amplifying the signal by applying a potential difference of 0.5-1 kV is carried out exclusively by building an appropriate electronic circuit. In this case, it is not necessary to cool this type of detectors. This leads to the possibility of their use in normal climatic conditions. The proposed design is also convenient for the organization and operation of field monitoring lightning detectors. The first experiment is planned to be carried out near the building of the branch of the Faculty of Physics and Technology in Smolyan. The faculty building is located at an altitude of 900 meters above sea level. In this case, the lightning discharge is much closer to the detectors than at sea level. The portability of the equipment makes it easy to carry and maintain in the field. In particular, in analogy to tornado hunters, they should be placed on the base of a car or a trailer for it.

The present paper consists of 1. Introduction, 3. Chapter, 5. Discussion and 6. Conclusion. Chapter 2 is devoted to the structure and evolution of the flow of γ-quants formed in lightning. Of particular interest is the γ-flare, a precursor of the lightning itself and its structure. Chapter 3 is about signal structure and its movement according to the electronic circuit and the method of its processing. Chapter 4 is devoted to spectral analysis of signals, building temporal correlations between currents at different wavelengths. In discussion, a comparative analysis of multichannel spectrographic of a hard and optical radiations has been carried out. Their importance and indispensability in monitoring of unique explosive processes in astrophysics and geophysics is emphasized. In the conclusion the main new results of the article are carried out. The design and methodological advantages of the simulation method for the design and manufacture of the necessary electronic components of a multichannel spectrograph are given.

The motion of a stream of protons, α-particles of positive ions, and the most common ions in a strong electric field with E is of particular interest. In lightning, the initial velocities of both the accelerated particles and the target molecules are close to thermal.

When an external field E is applied, the entire medium undergoes strong polarization, the effective binding energy of molecular electrons with shielded nuclei becomes smaller, and the medium begins to fill with free electrons. This process leads to the appearance of positive molecular ions and electrons in the flash heads.

The onset of ion motion is accompanied by elastic collisions with neutral molecules and atoms of the atmosphere. In elastic collisions with neutral atoms, atomic and molecular ions have a much higher energy transfer coefficient $\chi_{\alpha.\beta}$ than electrons. The same ratios affect the growth of ion velocities at the distances of their free paths.

As soon as the kinetic energy becomes comparable to the binding energy of molecular and atomic electrons, charge exchange reactions and detachment of electrons from parent atoms and molecules begin.

A further increase in velocity leads to a decrease in the cross section for the interaction of the ion current with the resting atoms of the atmosphere. Atomic and molecular current ions begin to maintain themselves in an ionized state.

The criteria of charge retention depending on the current velocity are described and systematized in detail in (Sigmund, 2014). Let the atomic number of the nucleus of the atom participating in the current Z_1 and the charge of its ion q_1,, the standard Bohr velocity $v_0 = c/137$ and its velocity v. Then, according to Bohr, in the hydrogen-like approximation, by replacing the nuclear charge by the effective charge Z_{1eff}, the following relation is satisfied

$$q_1 = Z_{1eff}\left(1 - exp\left(-\frac{v}{Z_{1eff}^{\frac{2}{3}} v_0}\right)\right) =$$

$$= Z_{1eff}\left(1 - exp\left(-137v/Z_{1eff}^{2/3}\mathrm{c}\right)\right). \qquad (2)$$

Figure 2 shows the ionization characteristics for hydrogen, helium, carbon, nitrogen and oxygen ions under lightning head conditions. When a sufficient velocity v is reached, a state of complete ionization is reached. The q_1 functions shown in the figure indicate zones of spectrum formation over a wide range for waves. In contrast to classical plasma, here a directed ion stream collides with atmospheric atoms that are practically at rest. And the cross sections of all the successive collision processes make it possible to estimate their intensities, which is important for planning an experiment.

In contrast to the differences in particle deceleration processes in the strong electric field of lightning, the acceleration of positive ions and electrons is observed. Figure 1 shows the results of calculations of the degree of ionization of atoms during such a movement. At high speeds, fully charged ions are formed. The velocities marked on the graphs correspond to the kinetic energies of the ions in the range 2.8 – 32 MeV. Collisions of ions with resting atoms of the atmosphere produce both induced

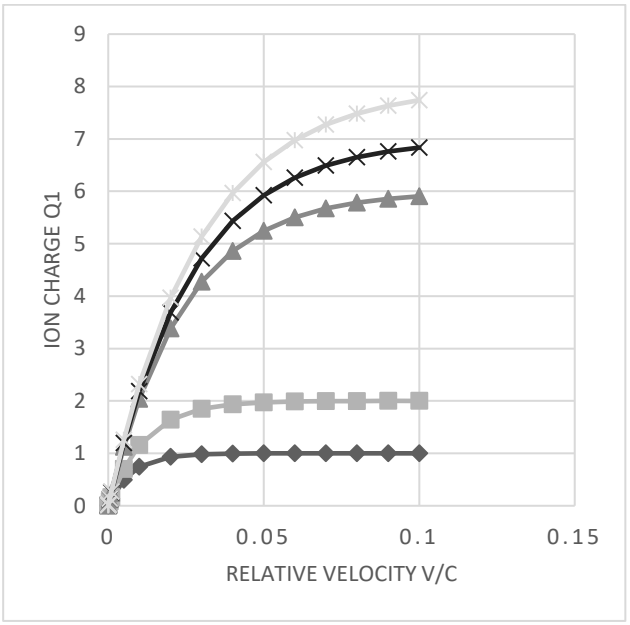

Figure 2: Ionization degree for elements Q1 for elements: ◊ – H, ▪ – He, Δ – C, X – N, * – O in lighting.

gamma rays and proton-excess nuclei. In any case, the appearance of a gamma-ray burst in the flash head is expected. Several μs before the onset of the optical phase of the discharge suggest that classical shock transitions do not manifest themselves in the optics. The developed detector covers the lightning spectra from optical to soft gamma radiation. Preliminary calculations of the total radiation losses show the highest information content in the marked region.

In 2017, slab γ-ray bursts were registered with the help of upgraded detectors installed at nuclear power plants after the well-known Fukushima accident. The registration of bursts coincided with the presence of a lightning storm in the vicinity of the nuclear power plant. The physical aspects of γ-burst formation have been considered in our work (Doikov D. & Doikov M., 2023, in press). Here we also discuss the structure and energy of a storm's γ-flares for modeling the detector's mode of operation. The fact that the building of the Branch of the Faculty of Physics and Technology is located at the altitude of 900 m is also very convenient for the sensor calibration experiment.

This leads to the fact that the detector is as close as possible to the source of γ-radiation. The source of γ-radiation of interest to us is located in the upper part of the lightning. In the so-called upper stage with lengths reaching 1 km. In this lighting current tube, the potential differences reach 10^8 V and the intensity of the electrical field is $(10^6 - 10^7)V/m$. The γ-spectra consists slab background continuous components and (0,511, 1,112) MeV emission line after collisions between accelerated electrons, protons and He ions (Doikov D. & Doikov M 2023, in press). The average statistical values of the characteristic time of formation of γ-flares are well known, which usually occur between 200 – 300 μs. The predicted flux of γ-quanta per 1 cm^2 of the detector surface varies from 100 to 1000 quanta

depending on the mutual distance between the detector CsPbBr3 and the lightning head.

This results in the detector being as close as possible to the source of the γ radiation. The source of γ-rays we are interested in is located in the upper part of the flash. In the so-called upper stage with lengths up to 1 km. In this lightning tube the potential differences reach 10^8 V and the intensity of the electric field is $(10^6 - 10^7)V/m$. The γ-spectra consist of continuous slab background components and the (0.511, 1.112) MeV emission line after collisions between accelerated electrons, protons and He ions (Doikov D.& Doikov M., 2023). The statistical averages of the characteristic γ-flaring times are well known, typically occurring between 200 and 300 μs. The predicted flux of γ quanta per 1 cm^2 of detector surface varies from 100 to 1000 quanta depending on the mutual distance between the detector $CsPbBr_3$ and the flash head.

Pulse reading and counting. Unlike optical radiation, the refractive index of γ and X-ray radiation in crystals is usually very close to 1. Then we can estimate the characteristic time of its motion in the crystal body as the ratio of quantum velocity to the thickness of the absorbing layer d, $\Delta\tau_{ch} \approx d/c \approx 3 \cdot 10^{-11} s$ This time is much smaller than all the other times considered before. The minimum of the ionization relaxation time $\Delta\tau_{ion}$_ion is in the power of $\Delta\tau_{ion} \approx 10^{-8} s$ and corresponds to the times of electron-hole pair formation. In this case, the impulse is a rare event and available for its single account. In other words, each quantum forms its own pulse. From Fig.1 for $E_\gamma = 0.511 MeV$ we have $N_{\gamma e} \approx 4{,}3 \cdot 10^5$. The $CsPbBr_3$ electron-hole lifetime τ is close to $10^{-5} s$. The driving velocity $v_d = \mu E \approx 50 \frac{cm^2}{s} \cdot 5{,}6 \cdot \frac{10^3 V}{cm} \approx 2{,}8 \cdot 10^5 cm/s$. Typical external potential differences are 500 V (Liu et al., 2022), (Doikov M., 2022).

The free path length of the electron-hole pairs in the perovskite semiconductor is $v_d \tau \approx 5{,}6\, cm$ Considering the accuracy of the determination of the carrier mobility in the considered semiconductor for the used energy range, we can conclude that the electron-hole recombination in our perovskite crystal CsPbBr3 is insignificant. It is important to conclude that the current pulls do not decrease, which is important to count the individual events. The pulling amplitude in these conditions we estimate from formula: $I = env_d S \approx 0{,}25 \cdot 10^{-6}$ A. In the case of heavy element semiconductors, we have avalanche breakdown. This type of breakdown is based on the effect of avalanche multiplication of carriers in the thickness of the p-n junction. At a certain value of the reverse bias voltage, the field strength in the p-n junction becomes so large that the minority carriers accelerated in it acquire sufficient energy to ionize the neutral atoms of the semiconductor in the junction. As a result of ionization, an avalanche increase in the number of carriers occurs, creating a reverse current. Avalanche breakdown is typically observed at reverse bias voltages on the order of hundreds of volts. It is typical of relatively thick p-n junctions where each of the minority carriers is present.

Note that an avalanche-like increase in the concentration of charge carriers in the form of electrons and the holes they leave behind leads to an increase in current strength. The drift velocity of the electron-hole pairs does not change significantly. This effect is limited because only the electrons in the outer valence shells of heavy elements have low binding energies. The neighboring valence shells already limit the flow of electrons into the conduction band. Most often we are dealing with outer d- or f-shell electrons.

Part of the energy contributed by the gamma quanta is converted to heat. The resulting shot thermal noise is responsible for a current of amplitude i:

$$i_n = \sqrt{\frac{4k_B T}{R}} \approx \frac{1.23}{\sqrt{R}} 10^{-10} A\,. \qquad (3)$$

Were R to be ohmic resistance of $CsPbBr_3$ crystal in normal room condition. From (Liu et al., 2022) $R \approx 10^{10} \Omega$. Relative currents of individual γ-quants depend on geometry and material properties of this crystal, which we get from Herst's equation in form:

$$\frac{I}{I_0} = \frac{\mu\tau V}{d}\left(1 - e^{-\frac{d^2}{\mu\tau V}}\right) \approx \frac{0.8}{d}\left(1 - e^{-\frac{d^2}{0.8}}\right). \qquad (4)$$

The saturation current I_0 depends on the thickness d and corresponds to the maximum γ-ray flux that does not change with the full current pulse. In the majority of practical cases μτ = 8·10^{-4} cm^2/V. V=500 –1000V. The maximum thickness d at present is close to 1 cm. Figure 3 shows the useful currents for different d.

The maximum current pulls from γ quantum with energy before 1 MeV are produced for crystal thickness d=1 cm. This means that the increase in crystal size must be controlled simultaneously by adjusting the product μτ and the free path of the electron-dot pairs. It was confirmed early on that $\lambda \approx 4.5\, cm$. If $d \leq \lambda$, carriers do not recombine on crystal defects and reach the anodic contact. Fulfillment of these conditions allows for high accuracy of recorded signals. That is, the dispersion of individual pulses reaches minimal values. The spectral resolution is maximal.

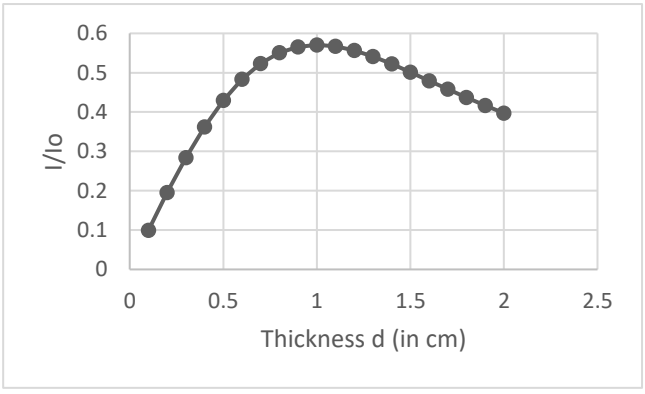

Figure 3: Dependence of the relative to saturation $\frac{I}{I_0}$ useful current from $CsPbBr_3$ crystal with thickness d (in cm).

Background and line γ-ray selections. During the study of the objects listed in this section, a low-amplitude continuous component of the γ spectrum appears. Emission lines appear against this background. Thus, guided by the physical characteristics of the process under consideration, it becomes possible to create a soft pulse processing program. We build the developed software into the pulse analyzer. According to Fig. 1, the pulse amplitude is related to the energy of the γ quantum. At the hardware level, we create a multichannel accumulator of pulses of the same amplitude. The time scale of these processes is limited only by the physical properties of the objects under study. Our research should be carried out in a monitoring mode. In this case, the software for processing the incoming information contains an algorithm for removing spurious signals and taking into account the dark current. To the above, we add that it is important to take into account and correct the natural radioactive background. Based on its average values, we can calibrate the detector used.

4. Emulation and selection of the type of signal from the pulse generator

The presence of heavy elements in the design of the detector leads to a sharp reduction of relaxation times during the formation of a current pulse of the useful signal. In this case, it is convenient to represent the signals as a Lorenz, Gaussian function. For sufficiently small widths and large amplitudes, the Dirac δ functions are used. On the other hand, amplitude, profile, and equivalent width are the most important spectroscopic characteristics for specialists. The physical mechanisms of γ line broadening before the advent of $CsPbBr_3$ γ detectors usually gave values within the error limits (Doikov D., 2022). The processing of the spectra is further complicated by the fact that the line broadening is much smaller than in the optical range. According to bench studies of the instrumental profile of semiconductors containing heavy metals, relaxation processes take much less time than those caused by real physical processes. The width of the instrumental profile in most cases is close to the natural profile of the γ-line. For the convenience of modeling the shape of the current pulse, we will use two profile formulas that are convenient for considering dissipative processes in semiconductors. In spectroscopy, such profiles are called Lorentz or Gaussian emission profiles. The Lorentz contour represents the evolution of some periodic processes in a dissipative physical system. In our case perovskite semiconductor.

$$P(\omega) = \frac{A_0^2}{(\omega-\omega_0)^2+(\gamma/2)^2} \quad . \qquad (5)$$

For ions is shown in the form:

$$P(\omega) = \frac{1}{\sigma\sqrt{2\pi}} e^{-\frac{(\omega-\overline{\omega_0})^2}{2\sigma^2}} \quad . \qquad (6)$$

The dispersion σ, frequencies ω, and $\overline{\omega_0}$ contain physical information about the equivalent width of the signal contour. We will interpret these values later in the next section.

Interference from useful signals. In classical signal theory, there are three main types of interference. These are:

1. Interference with a narrow frequency spectrum of signals caused by the operation of radio stations or sources of natural origin at close frequencies. Directed by the power supply.

2. Impulse interference, which is a chaotic sequence of impulses whose frequency is such that when the next impulse arrives, the processes caused by the previous impulses in the system are completed.

3. Fluctuation interference in the form of internal noise of transmission lines. Caused by the thermal motion of electrons in the conduction band of semiconductor devices. In our case, CsPbBr3 detectors.

These perturbations are such that the system's response to the next perturbation does not have time to fade before the next one arrives. Reactions from such a chaotic sequence are superimposed to form a continuous process. This phenomenon is often observed as a dark current.

We note that all these points are important to us. Point 1 is important for research in the presence of a densely packed, large number of spectral lines of atomic and molecular origin. Or when spectral studies are carried out near wavelengths occupied by strong resonance lines of atoms of the alkaline group of elements of the periodic table of elements of Mendeleev. The most interesting for us is point 2. Here, above the noise, we can expect to observe pulses of hard radiation quanta incident on the detector, quanta of the continuous γ-spectrum and noisy dark current. Of the considered signals represented by formulas (5) and (6), it is more convenient to use the Gaussian function to describe the time evolution of two successive pulses. Let us consider these pulses in the form of two Gaussian functions. With different mathematical expectations a_1, a_2 and variances σ_1, σ_2

$$f_1(t) = \frac{1}{\sqrt{2\pi}\,a_1} exp\left(-\frac{t^2}{2a_1^2}\right);\ f_2(t) = \frac{1}{\sqrt{2\pi}a_2} exp\left(-\frac{t^2}{2a_2^2}\right). \qquad (7)$$

The cross-correlation coefficient $k_{12}(\tau)$ describes the degree of magnitude in the resulting distribution, similar in meaning to the dispersion. $k_{12}(\tau)$ also represents the Gaussian distribution. If $a_{12}^2 = a_1^2 + a_2^2$ then the integral for calculating $k_{12}(\tau)$ has an exact solution and is useful for interpreting hard radiation spectral flux measurement data.

$$k_{12}(\tau) = \frac{1}{\sqrt{2\pi}\,a_{12}} exp\left(-\frac{\tau^2}{2a_{12}^2}\right). \qquad (8)$$

Thus, with a rapid increase in the flux of γ quanta, the indicator of the onset of detector saturation is the cross-correlation function $k_{12}(\tau)$ for each of the signal pairs. Considering that the detectors we design operate in the γ flare monitoring mode, the appearance of a non-zero cross-correlation function is a precursor of the flare itself. The single signal structure in the microscopic interpretation is the result of electron cloud motion in the conductive semiconductor zone. These electrons are injected after interactions between energetic hard radiation quants with heavy elements in the semiconductor (Fig. 1 and formula (1)). In the framework of relaxation time $\Delta\tau_{rel} \approx 10^{-9}s$ in the considered semiconductor, we must know that simultaneous backdown of more than 10^3 quants lead to

saturation of the detector system. The electronic architecture in Fig. 4 means that the hard radiation spectrograph works with overlapping signals. The degree of overlap is calculated from (8). If the inequality $k_{12}(\tau) \ll 1$ is satisfied, the splitting of the signal contours $f_1(t)$and $f_2(t)$ results from the formulas (7) for the free contour zone. In the opposite case, the increase of the dispersion leads to a decrease in the accuracy of the final spectra of the examined physical objects.

5. Registration of the magnetic field and distances from lighting

The directed motion of charged particles observed in lightning should generate local magnetic fields. If magnetic field detectors are placed near lightning, it is possible to measure magnetic field perturbations with sufficient accuracy. It should be noted that modern low-cost detectors available on the market make it possible to measure the local magnetic field with accuracy in the nanotesla range. On the other hand, for currents recorded by lightning, the calculated perturbations of the local magnetic field become comparable with the average magnetic field of the Earth. $\Delta B \approx \mu_0 I/r$. Where $\mu_0 = 4\pi \cdot 10^{-7} Hn/m$, I is the current of the charged particle (electron, proton or α particle). $I \approx 4 \cdot 10^4 - 10^5 A$, r is the distance between detector and illumination $r \approx 10^3 - 10^4$ m.

To determine the distance r from the lightning. A lightning-distance radiometer is suitable and available for sale on Internet platforms such as Amazon or others. In the frequency of radio waves, this device allows you to register lightning storms over long distances.

Thus, in field experiments, the optical and hard lightning spectra obtained as a result of work in monitoring mode can be compared with reliably fixed distances and local magnetic fields. In this case, we have an unambiguous picture of local physical processes in different parts of the lightning discharge.

6. Simulation in LabVIEW environment

First of all, we note that the present research is the pairing of two detectors within a single instrument. It can be called a prototype of a combined γ-optical telescope. We have divided the engineering and physical tasks of building a layout into two parts. The first part is devoted to the physical structure of a current pulse formed in a crystal under the action of an incident γ-quanta. A γ-quantum interacts with a crystal, and an optical quantum interacts with a CCD matrix. Both detectors are placed in the same mount and appear to distant objects as measuring instruments at the same point. In this case, signal synchronization requires taking into account the delay time caused by the operation of the devices involved in the simulation.

To simulate the operation of the detector, we will replace it with a standard pulse generator, and the operation of high-speed analog-to-digital converters with an integrator of individual signals. The resulting time spectrum is then displayed on the third device – an oscilloscope. The most suitable mode of operation of the pulse generator for us is the random signal generation mode. The point is that the processes we are considering take place in a highly turbulent medium. Within an acceptable energy interval, the generation of γ-quants is a random background process. The formation of a spectral emission line does not fit into the framework of such a concept. This means using a separate pulse generator where the waveform is given by a Gaussian function and simply means that it is more likely to be repeated. All of this is shown in Figure 2.

Noise suppression. The dark current of the crystal detector under normal conditions does not exceed 20 pA with a useful signal level of 80-100 pA. The first stage of signal amplification and signal registration is the creation of a significant potential difference in its working area. However, for crystals of the $CsPbBr_3$ type, a weak dependence of the dark current level on the temperature is observed. This simplifies the instrumental methods of noise treatment and brings them to the level of classical methods. Our discussion ends when we approach the saturation state of the detector. In this mode, these crystal degradation processes are already actively manifested. The level of uncontrolled noise increases here due to a decrease in the bandgap of the semiconductor under study.

The system consists of a charge-sensitive preamplifier, a shaping amplifier, and a multi-channel analyzer. Charges in the detectors are directed to the charge-sensitive preamplifier, accumulated on a capacitor, and then converted to voltage, which is then boosted to form a stepped voltage signal. The signal also passes through the preamplifier. One reason an amplifier is needed is to amplify the peak voltage resulting from the long attenuation of the signal's serial output from the preamplifier. An amplifier is therefore essential to accurately determine the height of each pulse. The technique involves modifying the attenuation curve into a narrower pulse shape while maintaining the height ratio of each pulse.

The circuit of a simple RC shaping amplifier is shown on the following page. It is a combination of a differentiator and an integrator. The differentiator acts as an upper pass filter, allowing only the high-frequency component to pass while blocking the constant component. Similarly, the integrator acts as a low-pass filter, allowing only the low-frequency component to pass, resulting in a gradually increasing slope. The output of the shaper amplifier is proportional to the signal level from the preamplifier, which is also proportional to the energy assimilated by the detector. It counts the number of pulses at different intervals and heights by applying a series of pulses with a specific shape to its input.

The multichannel analyzer (MCA) is an important device used in the production of gamma-ray spectra. It counts the number of pulses at different intervals and heights by applying a series of pulses with a specific shape to its input. The MCA consists of several channels, each with a window. If the height of an input pulse is within the window, the MCA records it as a single count in that channel. After a certain amount of time, the MCA produces a statistical output showing the number of samples and the corresponding channel number, which ultimately forms the final spectrum. The channel number is associated with both the pulse height and the gamma energy. By analyzing the spectrum against a known source, a correlation between energy and channel number can be made.

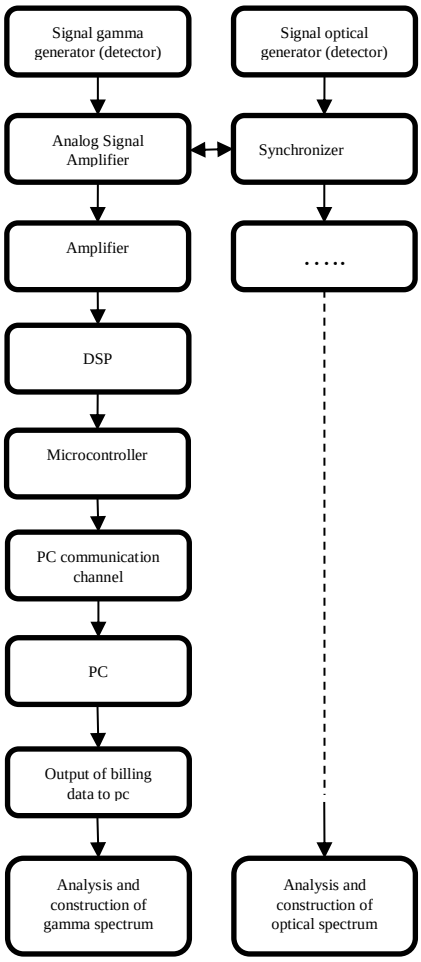

Figure 4: General block diagram of the current pulse motion and its analysis and simulation of the converted pulse

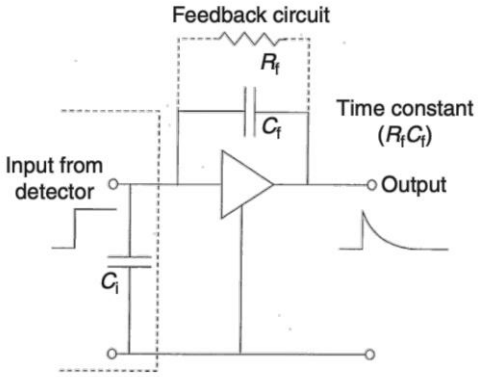

Figure 6: Preamplifier and signal structure (from Feng, 2020)

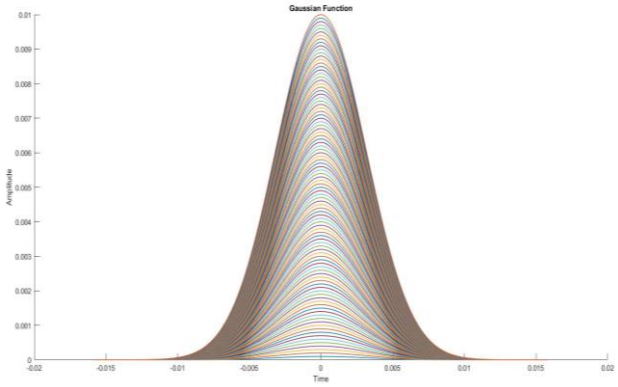

Figure 7: The original current pulls emulated from Palls generator before he enters into the preamplifier (the amplitude and dispersion parameters were configured with a dispersion of 10 μs and an amplitude ranging from 0.1 μA to 10 mA).

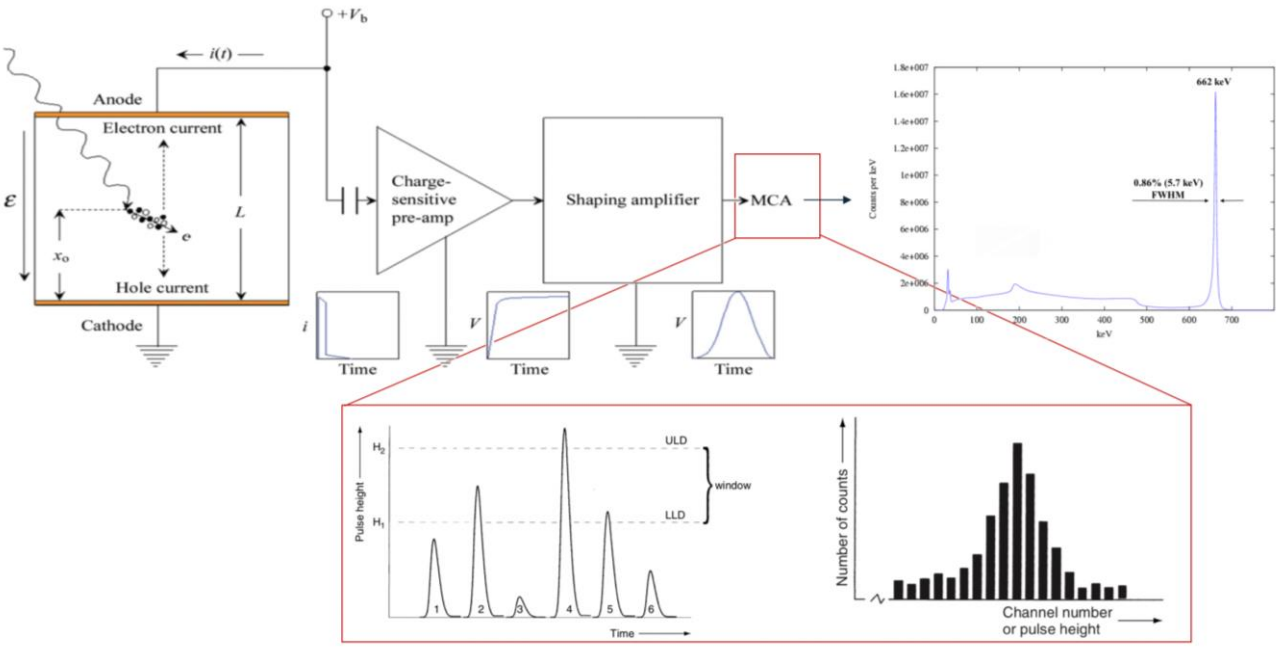

Figure 5: General block diagram of the analog current-potential pulse movement and analyses and simulation of the converted shapes (from Feng, 2020)

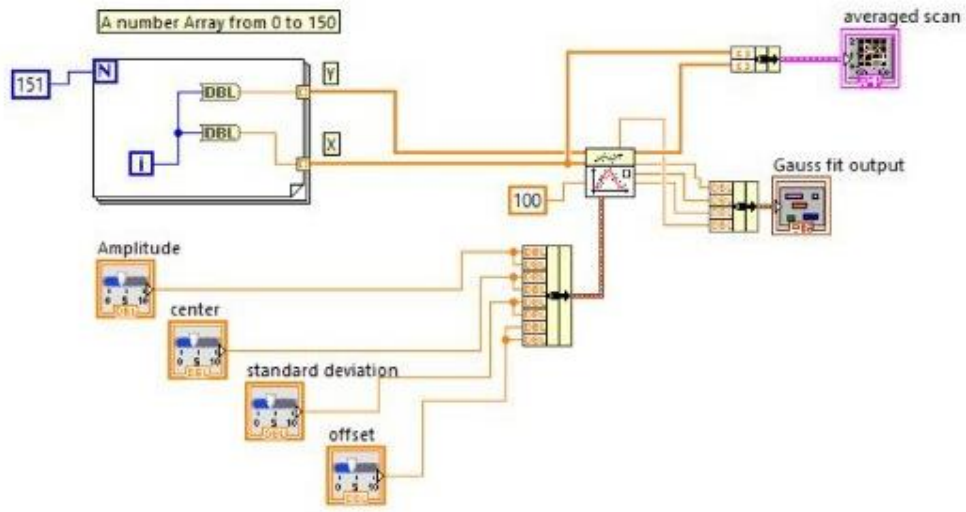

Figure 8: Used general block diagram of the current pulse movement and its analysis and simulation of the converted pulse.

In this paper, the optical part of the detector is referred to separately and considered in many works. For our case we used principles presented in (Rogalski & Bielecki, 2004). However, it is synchronized with the γ detector using a synchronizer. The studied physical processes are often accompanied by the formation of γ and optical spectra. Therefore, a stabilized time scale of the processes is crucial to avoid the loss of registration of the physical events. Our interest in considering the detection of two spectra simultaneously is also because peroxides can also be used to study optical spectra. However, well-available and highly sensitive optical spectrographs are now readily available and inexpensive for high-quality observations.

7. Discussion

The presence of heavy elements in the structure of a semiconductor allowed to solve several problems simultaneously, important solutions to practical problems of spectral diagnostics of fast processes of nuclear origin. First of all, it turned out that perovskite-based CsPbBr3 detector spectrographs are equally good for the construction of spectra of hard radiation and optical. In this paper, some of them are called binary detectors. The quantum states of the valence electrons and the characteristic times responsible for the filling of the conduction band by carriers under the influence of optical and γ-quanta are significantly different. However, they do not affect the formation of a current pulse from each γ- or optical quantum. In our opinion, both detectors should be placed in the same crystal body. The constructive part and the schematic diagram of the device were proposed by (Doikov M., 2022). The design features of binary detectors located in the body of a single crystal CsPbBr3 and the theory of current pulse formation will be the subject of our next work. In the meantime, we will consider the formation of the spectra of γ and optical radiation in single-crystal CsPbBr3 detectors.

8. Conclusion

Modern detector crystals made of the heavy elements Cs, Pb, and Br $CsPbBr_3$ make it possible to comprehensively solve the problems of studying fast processes in plasma, in which quanta of γ and optical radiation are formed simultaneously.

The ability to easily reconfigure the bandgap of a semiconductor makes it possible to preserve its multichannel nature.

Several physical objects have been considered that simultaneously generate gamma and optical spectra. correct processing of the signals coming from the final spectra. In the article, the characteristic times of formation of useful current signals in μs, pulse amplitudes in μA, and times between signals of tens of μs.

In the signal modeling phase, the above characteristics were used. Emulation was done using a signal generator in the LabVIEW environment. For high-speed ADCs presented in the same environment, the supply of the described signals from the detectors was tested.

We have found that the ADC processing of the applied current pulses in terms of amplitude and dispersion allows us to obtain the desired γ and optical spectra without loss and distortion of physical information.

Reference

Doikov D.N.: 2022, *Odessa Astron. Publ.*, **35**, 18.
Doikov M.D.: 2022, *Odessa Astron. Publ*, **35**, 24.
Doikov D.N., Doikov M.D.: 2023, *FAS*, **61**, in press.
Feng Y.: 2020, Master Degree Thesis. Univ. of North Carolina at Chapell Hill, 70 p.
Liu F., Wu R., Wei J., Nie W., Mohite A.D., Brovelli S., Manna L., Li H.: 2022, *ACS Energy Lett.*, **7 (3)**, 1066.
López C.A., María Consuelo Alvarez-Galván C.A., Hong B.-K., Martínez-Huerta M.V., Serrano-Sánchez F., Carrasco F., Castellanos-Gómez A., Fernández-Díaz M.T., Alonso J.A.: 2020, *ACS Omega*, **5 (11)**, 5931.
Ma W., Liu L., Qin H., Gao R., He B., Gou S., He Y., Ouyang X.: 2023, *Sensors*, **23**, 1.
Rogalski A., Bielecki Z.: 2004, *Bull. of the Polish Ac. Of Sciences. Technical Sciences*, **52**, No.1, 43.